Compressible viscous flow in slits with slip at the wall

Georgios C. Georgiou

Department of Mathematics and Statistics, University of Cyprus, Kallipoleos 75, P.O. Box 537, Nicosia, Cyprus

Marcel J. Crochet

Unité de Mécanique Appliquée, Université Catholique de Louvain, Bâtiment Euler 4-6, Avenue Georges Lemaitre, B-1348 Louvain-la-Neuve, Belgium

(Received 25 August 1993; accepted 13 January 1994)

Synopsis

We study the time-dependent compressible flow of a Newtonian fluid in slits using an arbitrary nonlinear slip law relating the shear stress to the velocity at the wall. This slip law exhibits a maximum and a minimum and so does the flow curve. According to one-dimensional stability analyses, the steady-state solutions are unstable if the slope of the flow curve is negative. The two-dimensional flow problem is solved using finite elements for the space discretization and a standard fully implicit scheme for the time discretization. When compressibility is taken into account and the volumetric flow rate at the inlet is in the unstable regime, we obtain self-sustained oscillations of the pressure drop and of the mass flow rate at the exit, similar to those observed with the stick-slip instability. The effects of compressibility and of the length of the slit on the amplitude and the frequency of the oscillations are also examined.

I. INTRODUCTION

Flow instabilities occurring during the extrusion of polymeric melts limit the output rates and are detrimental to the quality of the extrudate. They have thus received considerable attention in the past three decades [Petrie and Denn (1976); Piau *et al.* (1990); Denn (1992)]. The different surface defects can more easily be described by means of the flow curve (wall shear stress versus apparent wall shear rate or pressure drop versus volumetric flow rate). Kalika and Denn (1987) distinguish four flow regimes for low-density polyethylenes: (1) The *stable* regime below a certain critical throughput (or a critical stress of order 0.2 MPa), in which the extrudate surface is smooth. (2) The *sharkskin* regime above the critical throughput in which the extrudate surface shows a small-amplitude, high-frequency roughness (sharkskin or *surface melt fracture*). Kurtz (1984) noticed the coincidence of a change of slope of the log shear stress-log shear rate curves and the visual onset of sharkskin (loss of gloss). (3) The *stick-slip* (or spurt) regime above a second critical throughput in which periodic pressure and flow-rate fluctuations are observed, and the extrudate surface is characterized by alternating relatively smooth and sharkskin regions (*cyclic melt fracture*). The average stress reaches a maximum and then a minimum in this regime. (4) The *wavy* regime in which the extrudate exhibits wave-like distortions, usually of a helical kind (*gross melt fracture*).

The above classification may not be appropriate for other melts and is by no means universally accepted. Some investigators consider all the above instabilities not as distinct phenomena but as consecutive forms of melt fracture [Denn (1992)]. Piau and El Kissi (1992) found that at higher flow rates the stress reaches a second maximum and then a minimum. Also, at very high volumetric flow rates one would expect a rather chaotic regime with pronounced distortions of the extrudate surface, lack of periodicity, and eventually breakup of the extrudate [Pearson (1985); Piau *et al.* (1990)].

Agreement has yet to be reached as far as the origins and the mechanisms of the various types of melt fracture are concerned. Some investigators argue that the cyclic and gross melt fractures originate upstream in the die-entry region [Piau *et al.* (1990); Piau and El Kissi (1992)], whereas others believe that they only appear within the die (especially near the exit), associated with macroscopic slip at the wall, and they are most easily observed in extrusion through a long die [Denn (1990); Denn (1992)]. For the sharkskin defect, however, there appears to be a consensus, and it is considered as a purely exit phenomenon.

The possible mechanisms of instability have been the subject of debate. Constitutive instabilities and slip at the wall constitute the most popular explanations. Constitutive instabilities are caused either by changes of type of the governing equations or by multiplicities in the stress constitutive equation [Denn (1990)]. In examining the latter type of instability, some researchers considered constitutive models exhibiting a nonmonotonic (double-valued) steady shear response, like the Johnson–Segalman and the Doi–Edwards models, and carried out one-dimensional linear stability or numerical transient analyses showing that the steady-state solutions are unstable whenever the slope of the shear stress-shear rate curve is negative [McLeish and Ball (1986); Kolkka *et al.* (1988)].

The importance of constitutive instabilities, however, has been recently reconsidered by many rheologists [Pearson (1985); Denn (1990); Denn (1992)]. It is now more widely accepted that slip along the wall plays a crucial role in melt-flow instability. Extensive experimental results by Piau and his co-workers [Piau *et al.* (1990); Piau and El Kissi (1992)], and the recent findings of Hatzikiriakos and Dealy (1992a) from parallel plate and capillary experiments provide convincing evidence for the importance of slip.

Hatzikiriakos and Dealy (1992a) determined the slip velocity as a function of the wall shear stress using a modified Mooney technique. Reviews of the various slip velocity equations proposed in the literature are given by Hatzikiriakos and Dealy (1992b) and Denn (1992). At constant temperature, most of the proposed equations predict a power-law relation between the wall shear stress and the slip velocity. The equation proposed by Leonov (1990) exhibits a maximum and a minimum for the wall shear stress (as a function of the slip velocity); it is based on molecular considerations and contains parameters that are difficult to determine. Another empirical model exhibiting a maximum and a minimum was proposed by El Kissi and Piau (1989).

As early as in the mid 1960s, Pearson and Petrie (1965) considered the incompressible flow of Newtonian and power-law fluids in slits and tubes and carried out the linear stability analysis allowing slip at the wall by means of a generic slip equation relating the shear stress at the wall to the slip velocity. The Newtonian flow is unstable when the slope of the shear stress/slip velocity curve is negative. Pearson (1985) also provided an elementary explanation of the pressure oscillations observed with melt-flow instabilities in terms of bulk compressibility.

In this paper, we model the time-dependent compressible Newtonian flow in slits using an arbitrary slip equation relating the shear stress to the slip velocity and exhibiting a maximum and a minimum. This is the first step before attempting to simulate non-Newtonian flow instabilities, including the extrudate region and using a more realistic

slip equation. Of course, the idea is by no means new, but now available numerical techniques and computing power make such a simulation possible. The objective is to demonstrate the existence of a limit cycle due to the competition between compressibility and slip.

In our simulations, we consider the flow domain near the exit and we use the finite element method for the space discretization and a standard fully implicit scheme for the time discretization. In Sec. II, we present the governing equations and the slip equation together with some standard analytical solutions for relevant special flows. The numerical method is discussed in Sec. III; it is tested on some steady-state problems in Sec. IV. In Sec. V, we analyze time-dependent compressible flows with slip. In all the time-dependent runs, the volumetric flow rate at the inlet plane is kept constant by means of appropriate boundary conditions. The numerical results verify the importance of compressibility: it does not considerably affect the steady-state solutions but dramatically changes the flow dynamics. It is found that, under appropriate conditions, it is possible to generate self-sustained oscillations of the mass flow rate and of the pressure, which are typical of the stick-slip regime.

II. STATEMENT OF THE PROBLEM

A. Field and constitutive equations

Let ρ, p, $\mathbf{v}$, and σ be the density, the pressure, the velocity vector, and the stress tensor, respectively. The continuity and the momentum equations for time-dependent compressible viscous flow are as follows:

$$\frac{\partial \rho}{\partial t} + \nabla \cdot \rho \mathbf{v} = 0, \tag{1}$$

$$\rho \frac{\partial \mathbf{v}}{\partial t} + \rho \mathbf{v} \cdot \nabla \mathbf{v} - \nabla \cdot \sigma - \mathbf{f} = \mathbf{0}, \tag{2}$$

where $\mathbf{f}$ is the body force. For a Newtonian fluid, the stress tensor is given by

$$\sigma = -p(\rho)\mathbf{I} + 2\eta \mathbf{d} + (\kappa - \tfrac{2}{3}\eta)\mathbf{I} \nabla \cdot \mathbf{v}, \tag{3}$$

where $\mathbf{I}$ is the unit tensor, η is the viscosity, κ is the bulk viscosity, and $\mathbf{d}$ is the rate-of-deformation tensor, defined by

$$\mathbf{d} = \tfrac{1}{2}[(\nabla \mathbf{v}) + (\nabla \mathbf{v})^T], \tag{4}$$

where, as usual, $(\nabla \mathbf{v})^T$ is the transpose of $(\nabla \mathbf{v})$. For the bulk viscosity κ, we make the usual assumption that it is zero [Bird *et al.* (1960)].

The above equations are completed by a thermodynamic equation of state. Various essentially empirical equations of state can be found in the literature [Tadmor and Gogos (1979)]. Under the assumption of isothermal flow at low pressures, we resort to the first-order expansion:

$$\rho = \rho_0[1 + \beta(p - p_0)], \tag{5}$$

where

$$\beta = -\frac{1}{V_0}\left(\frac{\partial V}{\partial p}\right)_{p_0, T} \tag{6}$$

is the isothermal compressibility, assumed to be constant, ρ_0 and V_0 are the density and the specific volume at the reference pressure p_0 and T is the temperature. (A typical value for melt compressibility is 1.5×10^{-9} m^2/N [Tadmor and Gogos (1979)].) In most simulations of polymer flow, it is assumed that the fluid is incompressible. In our problem, however, compressibility is an essential ingredient of the flow dynamics as a mechanism for storing and releasing elastic energy in a limit cycle.

As a matter of fact, small changes in fluid density are normally accompanied by order-of-magnitude greater changes in viscosity. The pressure dependence of the viscosity is typically given by an expression of the form

$$\eta = \eta_0 \exp[\beta'(p-p_0)],$$

where η_0 is the viscosity at the (low) reference pressure p_0 and β' is a material parameter. For polyethylenes, reported values of β' range from 0.5 to 5×10^{-9} m^2/N [Hatzikiriakos and Dealy (1992a)]. At the present stage of our work, we do not take into account the pressure dependence of the viscosity.

B. The slip equation

We assume at the outset that the fluid slips along solid walls. The amount of slip is governed by a slip law that relates the shear stress on the wall to the relative velocity of the fluid with respect to the wall. For our present purpose, we need a slip law that is able to exhibit an unstable behavior. More precisely, the shear stress should show a local maximum for finite values of the relative velocity.

The form of the slip law used in our calculations is given as follows:

$$\sigma_w = \alpha_1\left(1+\frac{\alpha_2}{1+\alpha_3 v_w^2}\right)v_w, \tag{7}$$

where σ_w is the shear stress exerted by the fluid on the wall, v_w is the relative velocity of the fluid with respect to the wall, and α_1, α_2, α_3 are material parameters. We note that Eq. (7) is analogous to the expression relating the shear stress of a Phan-Thien-Tanner fluid (with an additional viscous component) to the shear rate in simple shear flow. The wall shear stress σ_w, as given by Eq. (7), exhibits a maximum if the dimensionless parameter α_2 is greater than 8. In Fig. 1, we plot σ_w vs v_w for different values of α_2, $\alpha_1 = 1$, and $\alpha_3 = 100$ (arbitrary units).

Let H and V denote a characteristic length and a characteristic velocity of the flow, respectively. To nondimensionalize the governing equations, we scale the lengths by H, the velocity by V, the pressure $(p-p_0)$ and the stress components by $\eta V/H$, the density by ρ_0, and the time by H/V. This scaling leads to five dimensionless numbers, the Reynolds number, Re, a compressibility number, B, and three numbers associated with the material parameters of the slip equation:

$$\mathrm{Re} \equiv \frac{\rho_0 V H}{\eta}; \quad B \equiv \frac{\beta\,\eta\,V}{H}; \quad A_1 \equiv \frac{\alpha_1 H}{\eta}; \quad A_2 \equiv \alpha_2; \quad A_3 \equiv \alpha_3 V^2. \tag{8}$$

In the sequence, we will exclusively use the resulting nondimensional equations and neglect the body force in the momentum equation.

It is known that, in extrusion of polymeric melts, $\mathrm{Re} \ll 1$. If we multiply the typical value for melt compressibility ($\beta = 1.5\times10^{-9}$ m^2/N) by the critical wall shear stress at the onset of instability (0.2 MPa), we find that a typical value of the compressibility number is $B = 0.0003$.

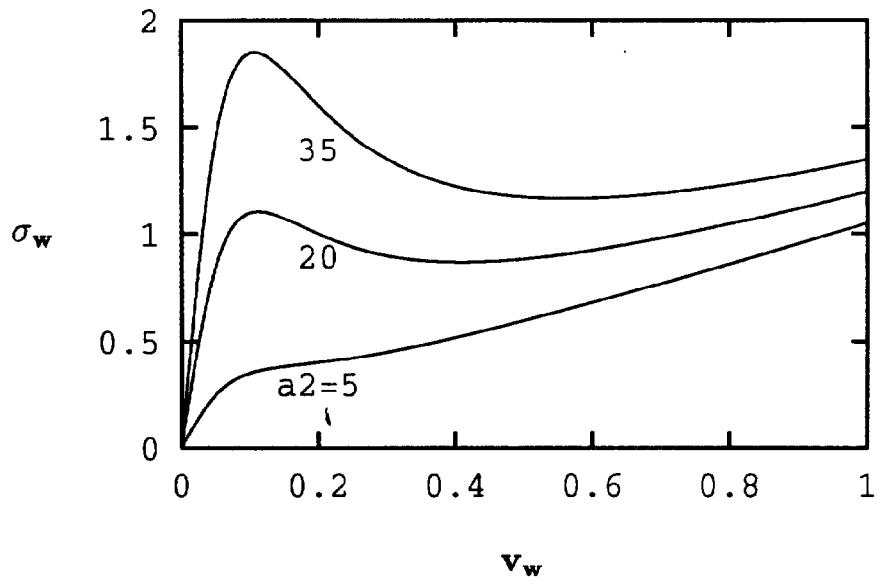

FIG. 1. Typical curves of the arbitrary slip law for different values of the dimensionless parameters of α_2, with $\alpha_1 = 1$ and $\alpha_3 = 100$ (arbitrary units).

C. Poiseuille flow

For later use, it is useful to record particular solutions of compressible plane Poiseuille flow with or without slip at the wall. H is taken as the half-width of the channel while V is the average inlet velocity.

We first consider the incompressible flow with the slip law given by Eq. (7). It is easy to show that the steady-state solution is given by

$$v_x = v_w - \tfrac{1}{2}\nabla P(1-y^2); \tag{9}$$

the fluid flows in the x direction, y is the lateral coordinate, and ∇P is the scalar pressure gradient. The force exerted by the fluid on the wall is precisely $-\nabla P$ and thus, in view of Eq. (7), we have

$$-\nabla P = A_1\left(1+\frac{A_2}{1+A_3 v_w^2}\right)v_w. \tag{10}$$

The volumetric flow rate for half of the channel (in nondimensional form) is given by

$$Q = v_w - \tfrac{1}{3}\nabla P. \tag{11}$$

We now consider the compressible flow with no slip at the wall. We can derive the analytical solution for Re = 0, with the assumption that the derivatives of the velocity across the slit (i.e., in the y direction) are much greater than in the direction of the flow (i.e., in the x direction). The flow domain is defined by $-\infty < x \leqslant 0$ and $-1 \leqslant y \leqslant 1$. The pressure p is set to zero at $x = 0$. For a compressible fluid, the pressure gradient is a function of x and so is the volumetric flow rate; the mass flow rate $\dot{M}$ is independent of x. One finds that

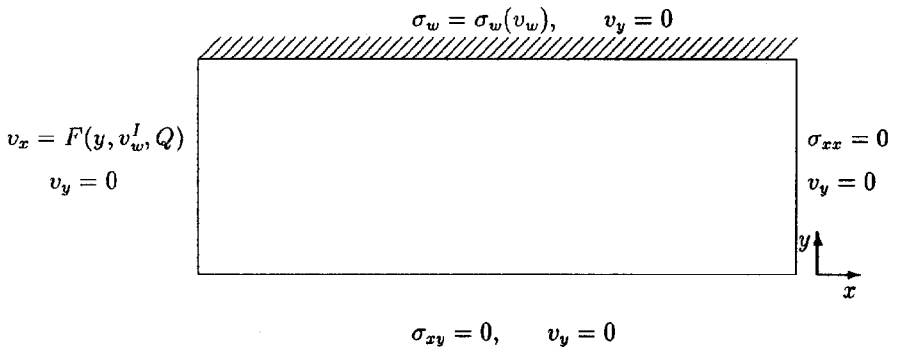

FIG. 2. Boundary conditions for compressible flow in a slit with slip at the wall.

$$p(x) = \frac{-1+\sqrt{1-6B\dot{M}x}}{B} \tag{12}$$

and

$$v_x = -\frac{1}{2}\frac{\partial p}{\partial x}(1-y^2) = \frac{3}{2}\frac{\dot{M}}{\sqrt{1-6B\dot{M}x}}(1-y^2). \tag{13}$$

We note that v_x is parabolic and its magnitude varies along x.

III. NUMERICAL METHOD

A. Galerkin formulation

In the present paper, we are interested in slightly compressible flow at very low values of the Mach number. We wish to solve the problem in terms of the velocity, the pressure, and the density as independent variables. The density can be eliminated, but we prefer to keep it as an additional unknown in order to have an easy-to-modify code able to handle more sophisticated equations of state.

The selection of the shape functions is an important issue in our formulation. Since we limit our investigation to low Mach and Reynolds numbers, we can use a straightforward extension of the standard velocity–pressure formulation for incompressible flow, i.e., biquadratic-velocity (P^2-C^0) and bilinear-pressure (P^1-C^0) elements. We use for the density the same low-order approximation as for the pressure. Fortin and Soulaimani (1988) have shown that such an element gives good results at low Mach and Reynolds numbers.

For time-dependent flow, we use the standard fully implicit (Euler backward-difference) scheme. As initial condition, we consider the steady-state solution corresponding to a volumetric flow rate Q at the inlet that we perturb by ΔQ at $t = 0$.

B. Boundary conditions

The boundary conditions for compressible flow in a slit with slip at the wall are shown in Fig. 2. Along the centerline, we have the usual symmetry conditions. Along the wall, the vanishing normal velocity constitutes an essential boundary condition. The slip ve-

locity v_w is unknown; however, we can assign a natural boundary condition in the tangential direction and express the tangential surface stress σ_w as a function of v_w on the basis of Eq. (7).

Since the flow is only slightly compressible, we assume that the velocity component tangent to the cross section vanishes at both the inlet and outlet planes. The numerical results show that this assumption is reasonable, at least for the relatively low compressibility numbers considered here. Moreover, we assume that at the outlet plane the total normal stress is zero, $\sigma_{xx} = 0$.

In order to calculate the inlet condition for v_x, let us assume that the density is a weak function of y, and that v_x is a parabolic function of y. The latter assumption is obviously true for the incompressible case. As shown in the previous section, it is also true for the compressible case, when inertia is neglected and the velocity gradients across the slit are much greater than in the direction of the flow. For planar flow, the velocity v_x at the inlet should satisfy the following conditions:

$$Q = \int_0^1 v_x \, dy, \quad \frac{\partial v_x}{\partial y} = 0 \quad \text{at } y = 0, \quad v_x = v_w^I \quad \text{at } y = 1,$$

where v_w^I is the unknown velocity at the wall. It turns out that

$$v_x = F(y, v_w^I, Q) = \tfrac{1}{2}(3y^2-1)v_w^I + \tfrac{3}{2}(1-y^2)Q. \tag{14}$$

The additional equation required for the calculation of the inlet velocity at the wall, v_w^I, is provided by the fact that v_w^I satisfies the slip law:

$$\sigma_w^I = -\left(\frac{\partial v_x}{\partial y} + \frac{\partial v_y}{\partial x}\right)_{y=1} = A_1\left(1 + \frac{A_2}{1+A_3(v_w^I)^2}\right)v_w^I.$$

Substituting from Eq. (14) gives

$$3(v_w^I - Q) = -A_1\left(1 + \frac{A_2}{1+A_3(v_w^I)^2}\right)v_w^I. \tag{15}$$

We should point out that v_w is a monotonic function of Q, provided that $A_2 < 8 + 24/A_1$; one can then easily calculate the velocity profile at the inlet for any value of Q.

IV. STEADY-STATE RESULTS

To study the effect of the mesh length and to check the validity of our boundary condition at the inlet, we have constructed meshes of two different lengths: $\Delta L = 5$ and 10. Different mesh refinements have also been considered in order to verify the convergence of the numerical calculations. The meshes were uniform in the direction of the flow and graded in the y direction. The mesh used in most calculations with $\Delta L = 5$ consisted of 25×7 elements.

A. No slip at the wall

We first check the validity of the boundary condition at the inlet by comparing the solutions obtained with meshes of different length. It turns out that up to $B = 0.1$, the calculated solution is practically independent of the mesh length. Note that for $B = 0.1$ the flow is markedly compressible and density doubles just five half-widths upstream the exit. Such density variations are obviously unrealistic and the runs for this extreme case are just used as a check to the numerical scheme and the assumptions we have made.

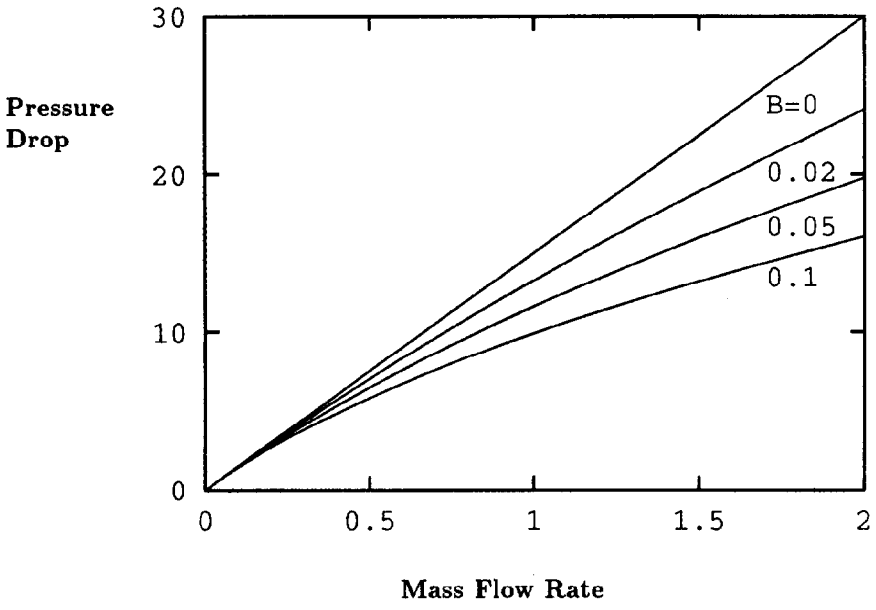

FIG. 3. Flow curves for different values of B; $\Delta L = 5$, no slip at the wall.

The flow curves (ΔP vs $\dot{M}$) for different values of B are plotted in Fig. 3. The pressure drop decreases as compressibility increases. Here, ΔP is the pressure drop along the wall (the pressure drop along the plane of symmetry is slightly lower). We chose to plot ΔP versus the mass flow rate $\dot{M}$ (and not versus the volumetric flow rate Q), because Q is not constant in the direction of the flow. We note, however, that at the exit $\dot{M} = Q$.

B. Slip at the wall

We now examine the effect of using slip at the wall. The numerical results are identical to their analytical counterparts given in Sec. II. In all the subsequent results we take $A_1 = 1, A_2 = 20$, and $A_3 = 100$. The flow curve for incompressible flow and $\Delta L = 5$ is given in Fig. 4. Due to the particular choice of A_2, the flow curve exhibits a maximum and a minimum. In the same figure, we show the combined effect of slip and compressibility. The maximum and the minimum of the flow curve move to the right, as compressibility increases.

V. TIME-DEPENDENT RESULTS

For the time-dependent results, we use as an initial condition the steady-state solution corresponding to the volumetric flow rate Q at the inlet that we perturb by ΔQ at $t = 0$. We wish to study the evolution of the mass flow rate and of the pressure drop.

A. Incompressible flow with slip and compressible flow without slip

Our time-dependent results for incompressible flow with nonlinear slip at the wall, show that the flow field gradually readjusts itself to the new steady state, without the appearance of any instability, even when the imposed volumetric flow rate is in the unstable regime.

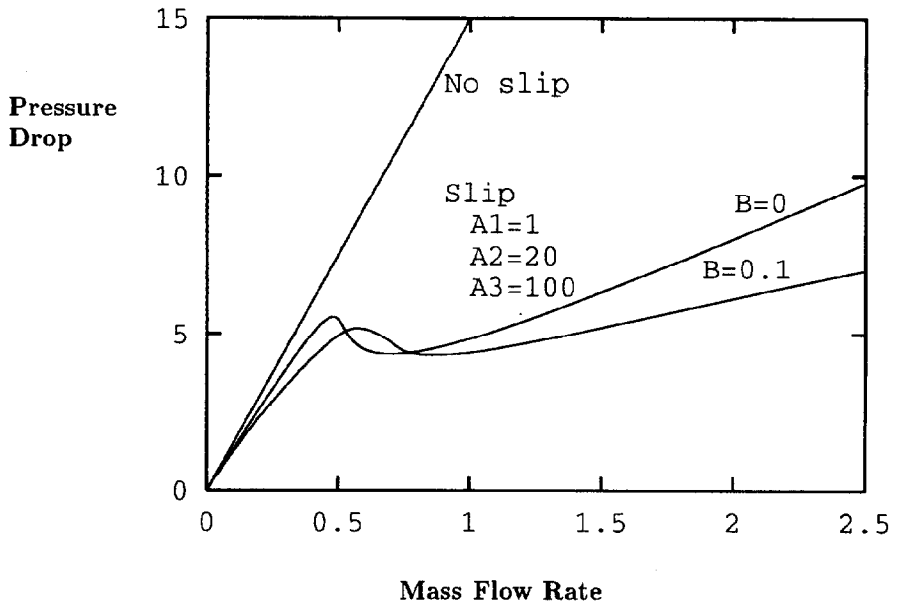

FIG. 4. Flow curves for flow with slip at the wall; $\Delta L = 5$.

Similarly, when the flow is compressible and no slip occurs at the wall, the perturbation of the volumetric flow rate in the entry section causes the readjustment of the flow field to the new steady state. The lack of unstable portions of the flow curve prevents the occurrence of oscillations.

B. Compressible flow with slip

First we examine the generation of self-sustained oscillations with the high value of the compressibility number $B = 0.1$, which is much larger than the values encountered in practice. Our purpose with this first example is to enhance the compressibility effects before using more realistic values of B. The Reynolds number is taken equal to 0.01. We start from a steady-state solution on the left stable branch and suddenly perturb Q to a value that corresponds to the right stable branch. The time-dependent solution is shown in Fig. 5. The trajectory of the time-dependent solution on the flow-curve plane is shown in Fig. 5(a). The initial state is located at point 1; the solution follows the path indicated by the arrow up to point 2 on the right stable branch. We observe simultaneous overshootings of the mass flow rate at the outlet [Fig. 5(b)] and of the pressure drop [Fig. 5(c)] before they converge to the new steady state. Again, if we perturb the volumetric flow rate to the previous steady-state value, we observe that the trajectories from the left to the right stable branch, and vice versa, do not coincide, and thus a hysteresis loop is obtained [Fig. 5(a)].

We now proceed to examine the time-dependent solutions when the imposed volumetric flow rate is in the unstable regime. We again consider the flow in a slit with $B = 0.1$ and $\mathrm{Re} = 0.01$. The volumetric flow rate is in the unstable regime and is suddenly decreased by 0.01%. The results for this run are shown in Fig. 6. This time, plotting the

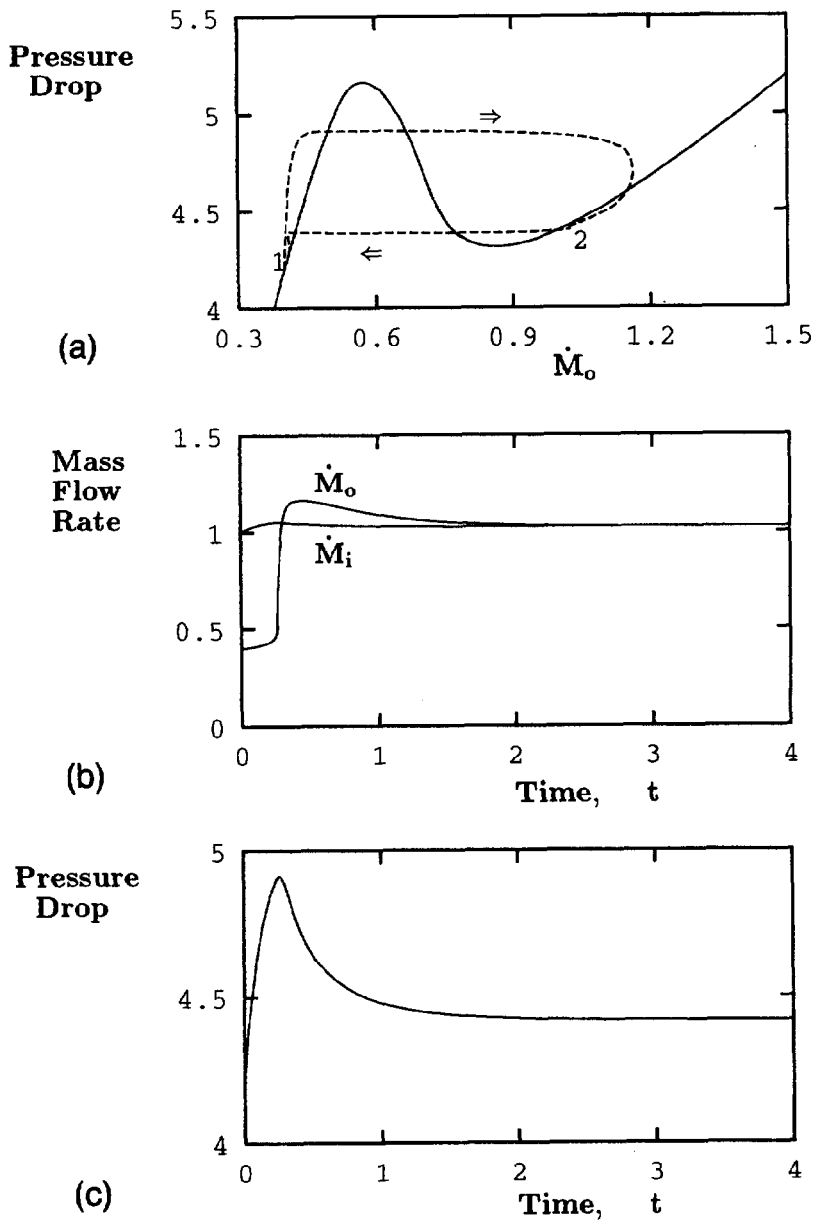

FIG. 5. Transient solution for compressible flow in a slit starting from a steady-state solution on the left stable branch and perturbing the volumetric flow rate to a value that corresponds to the right stable branch; (a) Trajectory of the solution on the flow-curve plane; (b) mass flow rates at the inlet ($\dot{M}_i$) and the outlet ($\dot{M}_o$); and (c) pressure drop; Re = 0.01, $B = 0.1$, and $\Delta L = 5$.

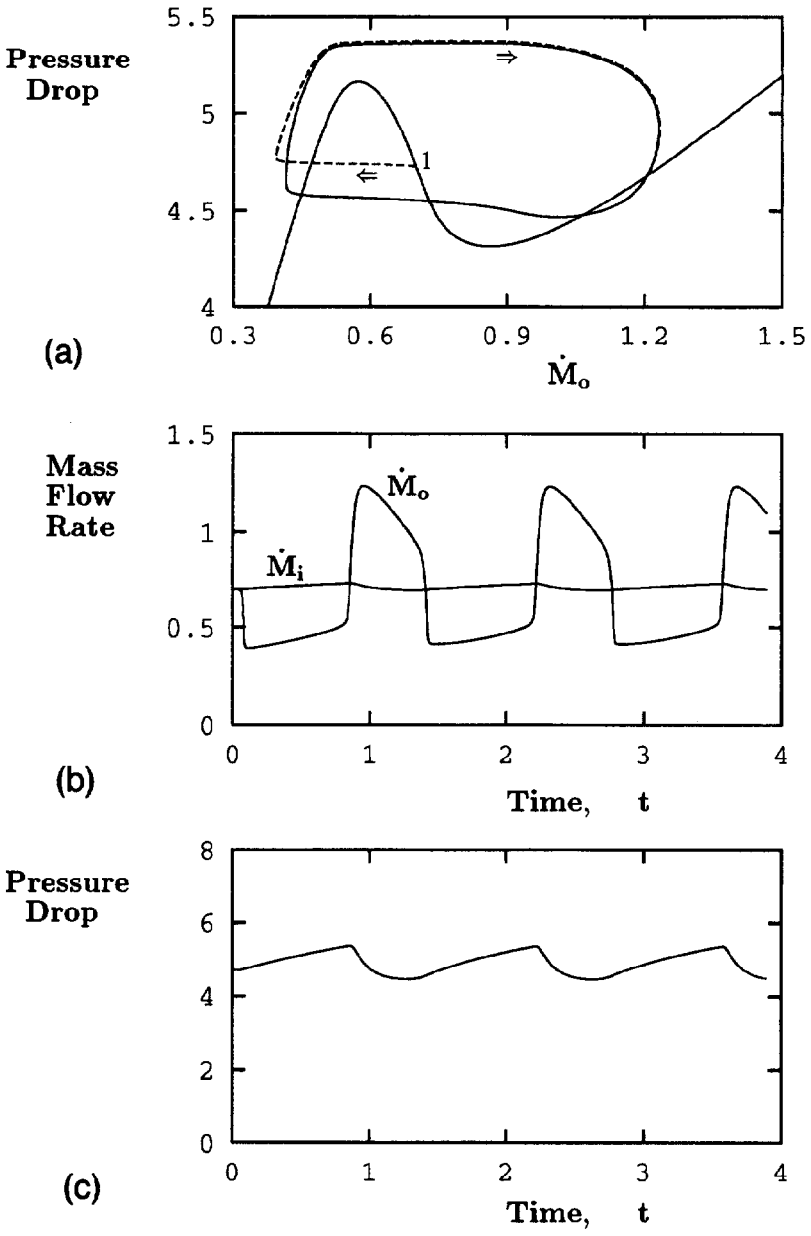

FIG. 6. Transient solution for compressible flow in a slit starting from a solution in the unstable regime that is slightly perturbed; (a) trajectory of the solution on the flow-curve plane; (b) mass flow rates at the inlet ($\dot{M}_i$) and the outlet ($\dot{M}_o$); and (c) pressure drop; Re = 0.01, $B = 0.1$, and $\Delta L = 5$.

pressure drop versus the mass flow rate at the outlet reveals the existence of a limit cycle [Fig. 6(a)]. The solution starts at point 1 and follows the arrow. As shown in Figs. 6(b) and 6(c), self-sustained oscillations of the mass flow rate and of the pressure drop, similar to those observed with the stick-slip instability, are obtained.

The solution jumps from the low- to the high-flow-rate stable regime, and vice versa, when some upper and lower critical values of the pressure drop (i.e., the shear stress) are reached, respectively. At the upper critical shear stress, slip becomes significant, whereas at the lower critical shear stress, adhesion to the wall is reestablished and the slip velocity becomes minimal. Note that these critical values do not coincide with the steady-state maximum and minimum values of the flow curve, and the limit cycle does not follow exactly the stable branches of the flow curve. The above mechanism was used by Hatzikiriakos and Dealy (1992b), who developed a model to simulate their time-dependent experiments. Their upper and lower critical values of the pressure drop, however, coincide with the extreme values of their experimental flow curve.

As mentioned earlier, the value $B = 0.1$ corresponds to highly compressible flow and thus to unusual conditions for polymer flows. Let us now consider the same flow conditions with values of B and of the same order as those encountered in practical applications. In Figs. 7 and 8, we plot the results for $B = 0.001$ and 0.0001 ($\mathrm{Re} = 0.01$ in all cases). We observe that as the fluid becomes less compressible, the frequency of the oscillations becomes higher and the amplitude of the mass flow-rate oscillations decreases, in contrast to that of the pressure-drop oscillations. The higher frequency may be attributed to the higher stiffness of the fluid in compression. At this point, we note that the amplitude and the frequency of the oscillations are intrinsically linked to the shape of the flow curve and thus to the form of the slip equation. The use of a realistic slip equation would, therefore, be in order if more meaningful results are to be obtained.

The dependence of the oscillations on the shape of the flow curve around the critical range is clearly seen when we increase the length of the mesh. In Fig. 9, we show the results obtained for $B = 0.0001$ and $\mathrm{Re} = 0.01$ using the longer mesh ($\Delta L = 10$). Comparing the numerical results with those with the shorter mesh in Fig. 8, we observe that the amplitudes of both the mass-flow-rate and the pressure-drop oscillations increase as ΔL increases. On the other hand, the frequency of the oscillations decreases. Here we should recall that our slip equation does not take into account any pressure effects.

VI. CONCLUSIONS

We have used the finite element method for the space discretization and a standard fully implicit scheme for the time discretization, in order to calculate time-dependent compressible Newtonian flow in slits with a nonlinear slip law at the walls. The slip law relates the shear stress to the relative fluid velocity at the wall and is of negative slope in some critical range of the slip velocity. Using this equation results in flow curves with two stable branches separated by an unstable negative-slope branch.

In the present paper, we have limited our results to the flow through a slit; we have recently extended our calculations to flows through tubes, and our observations remain entirely valid. Our two-dimensional calculations confirm earlier expectations: the combination of a nonlinear slip law with compressibility and inertia can generate self-sustained oscillations of the pressure drop and of the mass flow rate at the exit, similar to those observed with the stick-slip instability.

Of course, this work constitutes only a preliminary step toward the simulation of cyclic melt fracture. We have already linked our present simulations with the calculation of extrudate swelling; in a forthcoming paper, we will show the generation of wavy free

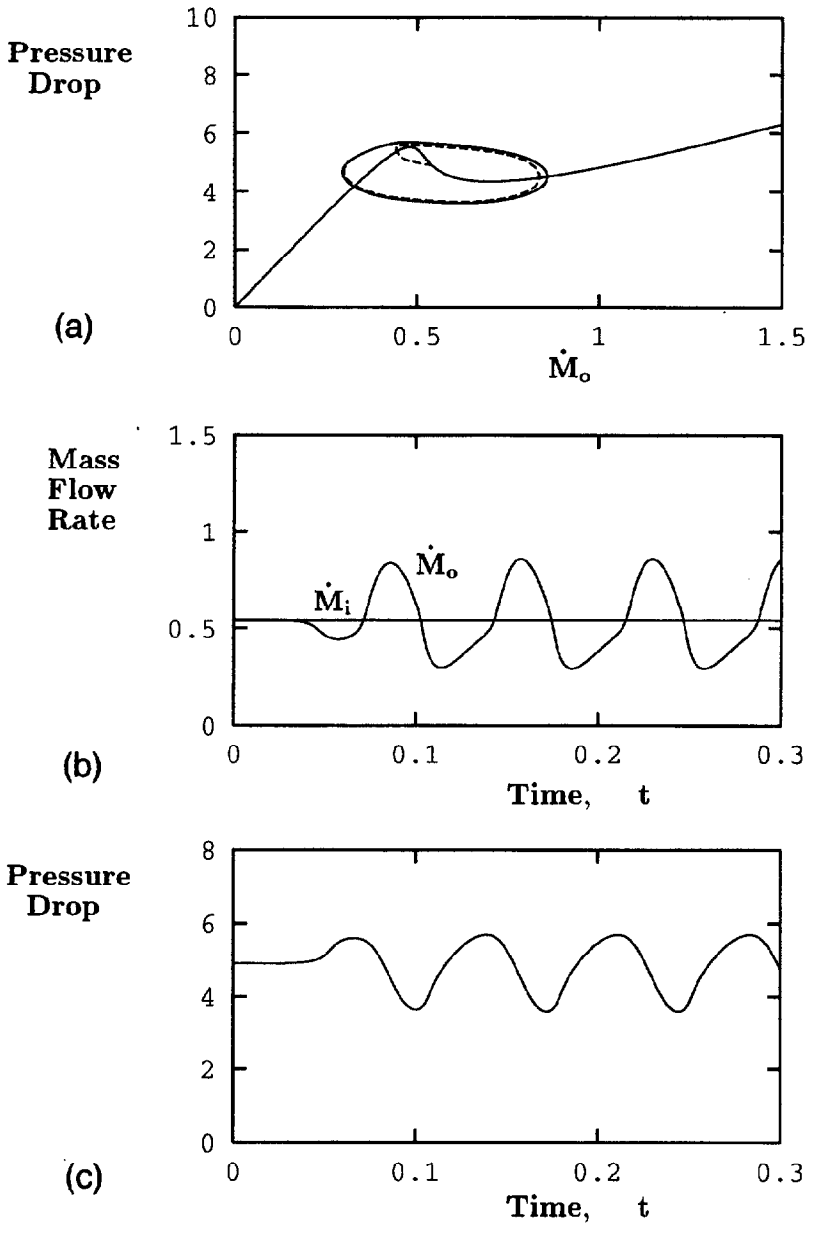

FIG. 7. Transient solution for $B = 0.001$ and Re = 0.01. (a) Trajectory of the solution on the flow-curve plane; (b) Mass flow rates at the inlet ($\dot{M}_i$) and the outlet ($\dot{M}_o$); (c) Pressure drop; $\Delta L = 5$.

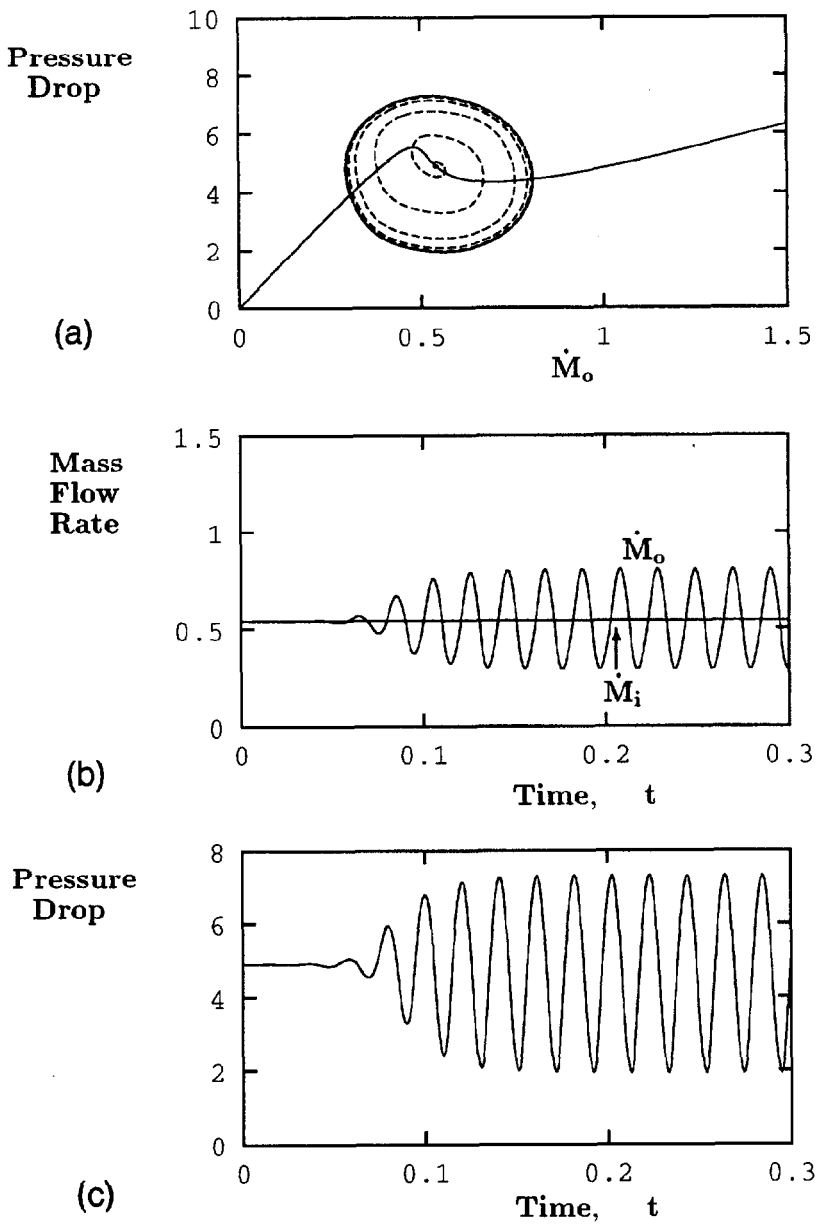

FIG. 8. Transient solution for $B = 0.0001$ and $\mathrm{Re} = 0.01$. (a) Trajectory of the solution on the flow-curve plane; (b) Mass flow rates at the inlet ($\dot{M}_i$) and the outlet ($\dot{M}_o$); (c) Pressure drop; $\Delta L = 5$.

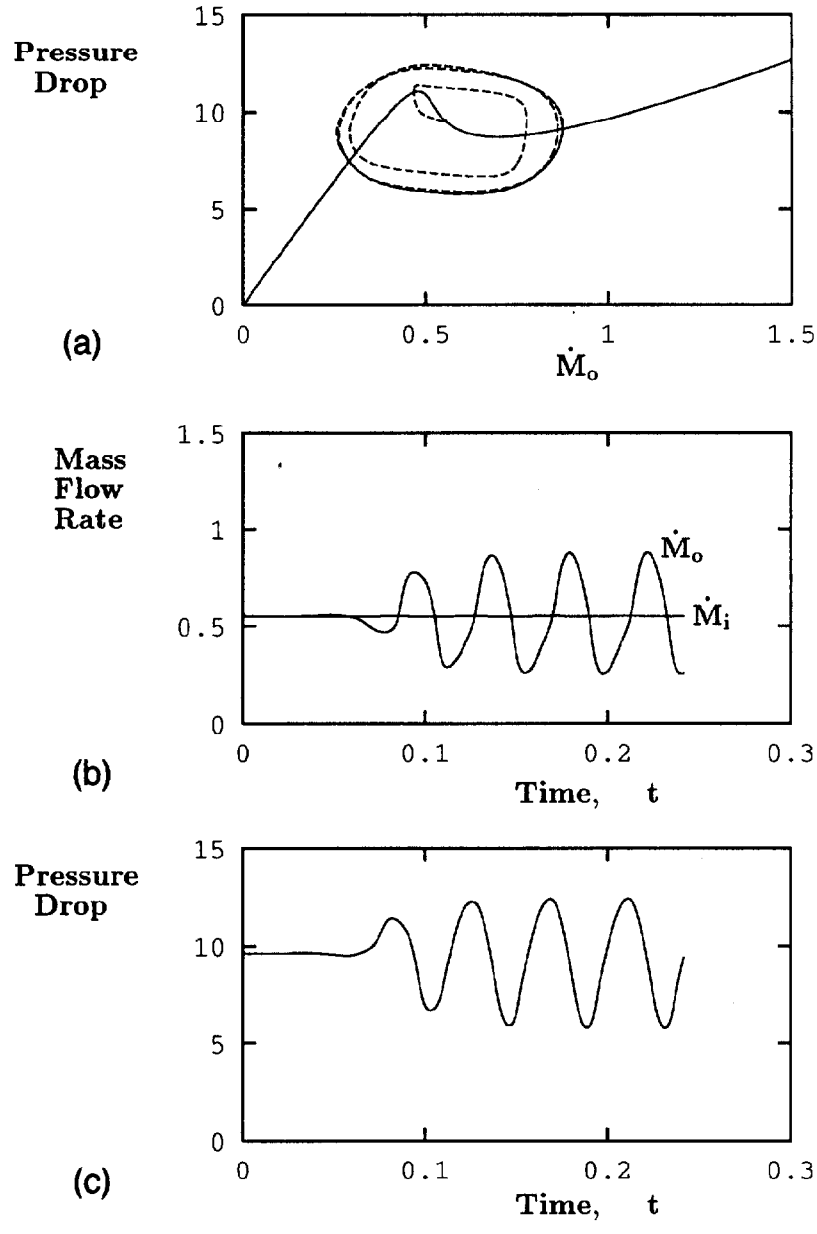

FIG. 9. Transient solution for $B = 0.0001$ and $\mathrm{Re} = 0.01$ in a longer slit ($\Delta L = 10$). (a) Trajectory of the solution on the flow-curve plane; (b) mass flow rates at the inlet ($\dot{M}_i$) and the outlet ($\dot{M}_o$); and (c) pressure drop.

surfaces at the exit of capillary tubes. However, any realistic simulation will need to take into account actual properties of polymer melts: a realistic slip equation based on experimental measurements, shear thinning, and viscoelasticity. The latter property would generate a second storage of elastic energy in the limit cycles and also guarantee a proper swelling ratio.

ACKNOWLEDGMENTS

The results presented in this paper have been obtained within the framework of Interuniversity Attraction Poles initiated by the Belgian State, Prime Minister's Office, Science Policy Programming.

References

Bird, R B., W. E. Stewart, and E. N. Lightfoot, *Transport Phenomena* (Wiley, New York, 1960).

Denn, M. M., "Issues in viscoelastic fluid mechanics," Ann. Rev. Fluid Mech. **22**, 13–34 (1990).

Denn, M. M., "Surface-induced effects in polymer melt flow," in *Theoretical and Applied Rheology*, edited by P. Moldenaers and R. Keunings (Elsevier, New York, 1992), pp. 45–49.

El Kissi, N. and J. M. Piau, "Ecoulement de fluides polymères enchevêtrés dans un capillaire, Modélisation du glissement macroscopique à la paroi," C. R. Acad. Sci. Paris **309**, Série II, 1989, pp. 7–9.

Fortin, M. and A. Soulaimani, "Finite Element Approximation of Compressible Viscous Flows," in *Computational Methods in Flow Analysis*, edited by H. Niki and M. Kawahara (Okayama Univ. of Science, Okayama, 1988), pp. 951–956.

Hatzikiriakos, S. G. and J. M. Dealy, "Wall slip of molten high density polyethylenes II. Capillary rheometer studies," J. Rheol. **36**, 703–741 (1992a).

Hatzikiriakos, S. G. and J. M. Dealy, "Role of slip and fracture in the oscillating flow of HDPE in a capillary," J. Rheol. **36**, 845–884 (1992b).

Kalika, D. S. and M. M. Denn, "Wall slip and extrudate distortion in linear low-density polyethylene," J. Rheol. **31**, 815–834 (1987).

Kolkka, R. W., D. S. Malkus, M. G. Hansen, G. R. Ierley, and R. A. Worthing, "Spurt phenomena of the Johnson–Segalman fluid and related models," J. Non-Newt. Fluid Mech. **29**, 303–335 (1988).

Kurtz, S. J., "Die geometry solutions to sharkskin melt fracture," in *Advances in Rheology*, edited by B. Mena, A. Garcia-Rejon, and C. R. Nafaile (Univ. Nat. Aut. Mex., Mexico City, 1984), Vol. 3, pp. 399–407.

Leonov, A. I., "On the dependence of friction force on sliding velocity in the theory of adhesive friction of elastomers," Wear **141**, 137–145 (1990).

McLeish, T. C. B. and R. C. Ball, "A molecular approach to the spurt effect in polymer melt flow," J. Polym. Sci. B **24**, 1735–1745 (1986).

Pearson, J. R. A. and C. J. S. Petrie, "On the melt-flow instability of extruded polymers," *Proceedings of the 4th International Rheological Congress*, 1965, Vol. 3, pp. 265–282.

Pearson, J. R. A., *Mechanics of Polymer Processing* (Elsevier, London, 1985).

Petrie, C. J. S. and M. M. Denn, "Instabilities in polymer processing," AIChE J. **22**, 209–236 (1976).

Piau, J. M., N. El Kissi, and B. Tremblay, "Influence of upstream instabilities and wall slip on melt fracture and sharkskin phenomena during silicones extrusion through orifice dies," J. Non-Newt. Fluid Mech. **34**, 145–180 (1990).

Piau, J. M. and N. El Kissi, "The influence of interface and volume properties of polymer melts on their die flow stability," in *Theoretical and Applied Rheology*, edited by P. Moldenaers and R. Keunings (Elsevier, New York, 1992), pp. 70–74.

Tadmor, Z. and C. G. Gogos, *Principles of Polymer Processing* (Wiley, New York, 1979).